



Methane coupling and hydrogen evolution induced by palladium-loaded gallium oxide photocatalysts in the presence of water vapor



Mizuki Ishimaru^a, Fumiaki Amano^{a,b,*}, Chiho Akamoto^a, Seiji Yamazoe^{b,c}

^a Department of Chemical and Environmental Engineering, The University of Kitakyushu, 1-1 Hibikino, Wakamatsu, Kitakyushu, Fukuoka 808-0135, Japan

^b Precursory Research for Embryonic Science and Technology (PRESTO), Japan Science and Technology Agency (JST), 4-1-8 Honcho, Kawaguchi, Saitama 332-0012, Japan

^c Department of Chemistry, Graduate School of Science, Tokyo Metropolitan University, 1-1 Hachioji-shi, Tokyo 192-0397, Japan

ARTICLE INFO

Article history:

Received 24 January 2021

Revised 18 March 2021

Accepted 22 March 2021

Available online 31 March 2021

Keywords:

Photocatalysis

Nonoxidative coupling of methane

Gallium oxide

Wide bandgap semiconductor

Adsorbed Water layer

ABSTRACT

Non-oxidative coupling of methane (NOCM, $2\text{CH}_4 \rightarrow \text{C}_2\text{H}_6 + \text{H}_2$) is a reaction that can directly produce ethane and hydrogen at the same time, and gallium oxide (Ga_2O_3) powder has been reported as an effective photocatalyst for NOCM at room temperature. In this study, we investigated the reaction conditions for Pd-loaded Ga_2O_3 photocatalysts to improve the production rate of C_2H_6 and H_2 . We found that the 0.1 wt% Pd/ Ga_2O_3 exhibited high selectivity of C_2H_6 (75.8%, carbon-based) under the conditions of steam reforming of methane. Photocatalytic NOCM seems to proceed in the presence of small amount of water. An increase in water vapor pressure ($P_{\text{H}_2\text{O}}$) was essential for the steady production of C_2H_6 and H_2 . The C_2H_6 production rate was $0.79 \mu\text{mol min}^{-1}$ for 50 mg of Pd/ Ga_2O_3 powder at $P_{\text{H}_2\text{O}} = 3.6 \text{ kPa}$. The apparent quantum efficiency (AQE) for C_2H_6 production was 5.1%, which is much higher than that of conventional photocatalytic NOCM in the absence of water vapor. The importance of water adsorbates on the photocatalyst surface was suggested by water vapor adsorption isotherm and Fourier transform infrared (FT-IR) spectroscopy. It is revealed that multilayered water molecules adsorbed on the photocatalyst surface play a role as a reaction field that promotes the dehydrogenative coupling of CH_4 .

© 2021 Elsevier Inc. All rights reserved.

1. Introduction

Methane (CH_4) is of considerable interest as energy resources due to the enormous amounts of unconventional natural gases such as shale gas and methane hydrate [1,2]. It is desired to use CH_4 more effectively as a carbon resource for chemicals as a substitute for petroleum [2,3]. There are indirect catalytic processes that convert CH_4 into chemical products, but overall energy efficiencies are not high because of the stepwise thermal reactions [4]. Therefore, single step (direct) conversion of CH_4 into chemical products such as C2 hydrocarbons (ethane and ethylene) is desirable. Oxidative coupling of methane (OCM), which activates CH_4 at high temperatures in the presence of oxygen and converts it to C2 hydrocarbons in a single step, has been investigated as the most potential catalytic method [5,6]. However, there are problems such as the sequential oxidation of the target molecule to CO_2 at high temperatures and the carbon deposition causing catalyst deactiva-

tion [5]. To solve these problems, a single-step process that activates CH_4 at lower temperatures is considered necessary.

One way to activate CH_4 at low temperatures is to use heterogeneous photocatalysts [7]. The photocatalysts excited by light energy proceed uphill reactions with reaction Gibbs energy $\Delta_r G > 0$ even at room temperature [8]. Photoexcited electrons (e^-) and hole (h^+) generated in semiconductor materials such as metal oxide particles induce reductive and oxidative reactions on the solid surface. Although the photocatalytic reaction mechanisms have not been fully understood, many solid photocatalysts have been reported for CH_4 conversion reactions [9,10]. Photoelectrochemical CH_4 conversions using semiconductor electrodes have also been investigated, but there are few reports [11,12].

Photocatalytic non-oxidative coupling reaction of methane (NOCM, $2\text{CH}_4 \rightarrow \text{C}_2\text{H}_6 + \text{H}_2$) can convert CH_4 to ethane and hydrogen in a single step at room temperature in the absence of oxidants such as oxygen and water [9,10]. Many heterogeneous photocatalysts have been developed for NOCM [9,10,13–17]. Wang and Zhang et al. reported that 2 wt% Pt-loaded and Ga-doped $\text{TiO}_2\text{-SiO}_2$ photocatalyst showed CH_4 conversion of 6.24% and C_2H_6 selectivity ($S_{\text{C}_2\text{H}_6}$) of 90.1% (on molar carbon basis) in a batch reactor under ultraviolet (UV) light irradiation [13]. However, the apparent quantum efficiency (AQE) was very low, $1 \times 10^{-4} \%$, a

* Corresponding author at: Department of Chemical and Environmental Engineering, The University of Kitakyushu, 1-1 Hibikino, Wakamatsu, Kitakyushu, Fukuoka 808-0135, Japan.

E-mail address: amano@kitakyu-u.ac.jp (F. Amano).

wavelength of 350 nm. Ordonsky and Khodakov et al. reported a stoichiometric photoreaction with AQE of 3.5% at 362 nm and $S_{C_2H_6}$ of 90% on TiO_2 photocatalyst loaded with silver ions and heteropoly acids (HPW) [14].

Gallium oxide (Ga_2O_3), which is a wide bandgap semiconductor ($E_g = \sim 4.4$ eV), has also been reported as photocatalysts that can promote NOCM under UV light irradiation [15,17]. Yoshida et al. reported NOCM with a CH_4 conversion rate of $0.5 \mu\text{mol g}^{-1} \text{h}^{-1}$ and AQE of 0.01% at 254 nm using a Ga_2O_3 photocatalyst [15]. They also reported that the loading of 0.5 wt% Pd cocatalyst increased the C_2H_6 formation rate ($R_{C_2H_6}$) of bare Ga_2O_3 three times [17]. The ratio of C_2H_6 to H_2 produced was 0.96, suggesting that NOCM is proceeding with high selectivity with few byproducts. However, the $R_{C_2H_6}$ and AQE were not high in the NOCM system using Ga_2O_3 -based photocatalysts. Therefore, it is necessary to improve the photocatalytic activity for NOCM dramatically.

Photocatalytic H_2 production by water splitting is known to be enhanced by the presence of CH_4 because of the progress of photocatalytic steam reforming of methane (photo-SRM), defined as the stoichiometric reaction of $CH_4 + 2H_2O \rightarrow CO_2 + 4H_2$ [18,19]. For photo-SRM, we found that Pt cocatalyst-loaded Ga_2O_3 photocatalyst (Pt/Ga_2O_3) shows not only a high rate of H_2 production but also a high $R_{C_2H_6}$ when methane partial pressure (P_{CH_4}) is high [20]. $R_{C_2H_6}$ increased monotonically with the increase in P_{CH_4} and reached $35 \mu\text{mol h}^{-1}$ for 50 mg of Pt/Ga_2O_3 at $P_{CH_4} = 300$ kPa. The $S_{C_2H_6}$ was 67% on a carbon basis, which indicating that photocatalytic NOCM partly proceeds under the condition of photo-SRM with water vapor. Based on the kinetic analysis and ESR measurement, we proposed the reaction mechanism via hydroxyl radical ($\bullet OH$) for C_2H_6 production by Pt/Ga_2O_3 photocatalyst in the presence of water vapor as follows [20].



Yu and Li et al. reported direct production of C_2H_6 and H_2 in a gas-liquid-solid system using Pt/TiO_2 photocatalysts suspended in water [21]. The byproducts were CO_2 and CO , and $S_{C_2H_6}$ was 61.7%. The AQE in H_2 production was 4.7% at a wavelength of 254 nm. They also reported that Pd/TiO_2 photocatalyst reduced AQE to 2.83% but improved $S_{C_2H_6}$ to 72.6% [22]. Yoshida et al. also reported that Pd cocatalyst was useful for NOCM among various metals (Pt, Pd, Ag, Ni, Fe, Zn, In, Rh) [17]. These reports suggest that Pd cocatalysts are more advantageous for C_2H_6 production than Pt cocatalyst.

In this study, we investigated the characteristics of the Pd/Ga_2O_3 photocatalyst using a flow reactor to improve the amount of C_2H_6 produced in the CH_4 conversion reaction in the presence of small amount of water. The Pd cocatalyst was loaded by the impregnation and the photodeposition methods. We examined the difference between Pt and Pd and the effect of the amount of Pd loading. Then, we investigated the effects of photocatalytic conditions such as water vapor pressure (P_{H_2O}), P_{CH_4} , light intensity, and reaction temperature. The dependence of $R_{C_2H_6}$ on P_{H_2O} and

reaction temperature suggested the importance of water adsorption on the photocatalytic surface. Therefore, we measured Fourier transform infrared (FT-IR) spectroscopy and water vapor adsorption isotherm to discuss the effect of water molecules adsorbed on the photocatalyst surface. We also compared the $R_{C_2H_6}$ in the presence of water vapor and liquid water.

2. Experimental method

2.1. Preparation of Pd/Ga_2O_3 photocatalysts

Ga_2O_3 powder (purity 99.99%) was obtained from Kojundo Chemical Laboratory. The BET specific surface area (S_{BET}) was $9.9 \text{ m}^2 \text{ g}^{-1}$ from the N_2 adsorption isotherm measurement.

The Pd cocatalyst was loaded by impregnation method according to the following procedure. Palladium chloride ($PdCl_2$) aqueous solution and deionized water (600 μL) were mixed with 1.5 g of Ga_2O_3 powder dried at 100 °C for 1 h. The sample was dried again at 100 °C for 1 h to obtain $Pd(\text{Imp})/Ga_2O_3$ powders. The loading amount was 0.1 wt% as Pd metal for Ga_2O_3 .

We carried out the photodeposition method according to the following procedure. Ga_2O_3 powder, 2.0 g, was added to a mixed solution of 10 vol% ethanol (180 mL of water, 20 mL of ethanol) and a $PdCl_2$ solution and ultrasonicated for 5 min. The loading amount was 0.1 wt% or 0.5 wt% Pd for Ga_2O_3 . After stirring with a magnetic stirrer for 30 min in the dark, UV light was irradiated by a 40 W low-pressure mercury lamp (ASM401N, Asumi Giken) for 1 h from the top of the beaker with magnetic stirring. Then, Pd/Ga_2O_3 particles were precipitated by centrifugation for 10 min and washed with 200 mL of deionized water under ultrasonication for 5 min. The precipitate was dried at 100 °C for 1 h to obtain a $Pd(\text{PD})/Ga_2O_3$ powder.

2.2. Photocatalytic reaction in a flow reactor

We carried out photocatalytic CH_4 conversion reactions using a fixed-bed flow reactor with an irradiation area of 25 cm^2 (Fig. S1). Photocatalytic powder, 50 mg, was applied onto a glass substrate using deionized water, dried at room temperature, and placed in a stainless-steel reactor (volume $25 \text{ cm}^2 \times 0.025 \text{ cm}$). CH_4 gas with water vapor was continuously supplied at a flow rate of 20 mL min^{-1} at room temperature of 25 °C. The P_{H_2O} was measured using a dew point transmitter for high humidity environments (EE33, Tekne). A 40 W low-pressure mercury lamp (ASM401N, Asumi-Giken) was used as the light source for deep UV light irradiation. The incident light intensity (I_0) was measured by a photometer (H9535-254, Hamamatsu Photonics) and 14 mW cm^{-2} at a wavelength of 254 nm. The reaction temperature was controlled by an electronic cooler (HMC-17F-2700, Hayashi-Repic) installed the bottom of the stainless reactor. When the cooler was set to 25.0 °C, the temperature of the fixed bed was increased to 27.0 °C under UV light irradiation. The saturated vapor pressure is 3.56 kPa at 27.0 °C [23]. The stainless-steel tubes connected to the reactor were warmed by ribbon heater to prevent water vapor's condensation. The reactants and products were analyzed by gas chromatography using packed columns (GC-8A with MS-5A, Shincarbon ST, and Polapak-Q, Shimadzu). H_2 was quantified by a thermal conductivity detector (TCD) with an argon carrier. CO_2 and CO were quantified by TCD with a helium carrier. Lower hydrocarbons such as C_2H_6 and C_3H_8 were quantified by a flame ionization detector (FID) with a nitrogen carrier.

The AQE was calculated as the ratio of the number of electrons consumed for the photocatalytic reaction to the number of incident photons using the following equation.

$$\%AQE = \frac{R_p \times n_e \times N_A}{(I_0 \times A \times 60 [s \text{ min}^{-1}] / (hc/\lambda))} \times 100 \quad (6)$$

where R_p , n_e , N_A , I_0 , A , h , c , and λ stand for the rate of molecule production (in mol min^{-1}), the number of electrons involved in the reaction, the Avogadro constant, light irradiance (in W cm^{-2}), irradiation area ($A = 25 \text{ cm}^2$), the Planck constant, the speed of light, and the wavelength of incident light ($\lambda = 254 \text{ nm}$). The AQE for H_2 was calculated using $n_e = 2$ assuming a two-electron process (Eq. 3).

2.3. Characterization of photocatalyst powders

X-ray diffraction (XRD) pattern was measured on a SmartLab diffractometer (Rigaku) using $\text{Cu K}\alpha$ radiation. Transmission electron microscopy (TEM) image was obtained using a JEM-3010 (JEOL) to observe the particles fixed on a microgrid. For scanning electron microscope (SEM) image, JSM-7800F (JEOL) was used to observe the particles fixed on the surface of carbon tape. The diffuse reflectance UV–visible spectrum was measured using a UV2600 spectrophotometer with an ISR-2600Plus integrating sphere accessory (Shimadzu) using barium sulfate as a reference sample.

The diffuse reflectance spectrum of FT-IR was measured using IRSpirit-T (Shimadzu) with a diffuse reflection chamber HC1000 (ST Japan) under humid CH_4 flow of 20 mL min^{-1} . An aluminum mirror was used as a reference sample. Water vapor adsorption and desorption isotherm was measured at $25 \text{ }^\circ\text{C}$ using a BELSORP-max (MicrotracBEL). The Ga_2O_3 powder (1.0 g) was evacuated at $200 \text{ }^\circ\text{C}$ for 2 h before the measurement. Electron paramagnetic resonance (EPR) spectrometry was performed on Magnetech ESR5000 (Bruker) at room temperature. The Pd(Imp)/ Ga_2O_3 powder (20 mg) was dispersed in an aqueous solution of 5,5-dimethyl-1-pyrroline-N-oxide (DMPO, 0.1 mol L^{-1}) as a radical trapping agent. The suspension was irradiated by UV light emitted from a 200-W mercury–xenon lamp (L9588-02A, Hamamatsu Photonics). The X-band EPR parameters were magnetic field of 330–340 mT, modulation amplitude of 0.1 mT, modulation frequency of 100 kHz, and microwave power of 10 mW.

The X-ray absorption fine structure (XAFS) of the Pd K-edge was measured at the beamline BL01B1 of the SPring-8 facility (Japan Synchrotron Radiation Research Center, Hyogo) with a Si (311) double-crystal monochromator at room temperature. The reference samples were measured by the transmission method using ionization chambers, and the photocatalyst samples were measured by the fluorescence method using a 19-element germanium solid-state detector. The XAFS spectrum was analyzed using xTunes software [24]. The χ spectrum as a function of photoelectron wavenumber k was weighted by k^3 , and Fourier transformed in the range of $k = 3.0\text{--}15.8 \text{ \AA}^{-1}$. The R range of $1.4\text{--}2.8 \text{ \AA}$ was inverse Fourier transformed and curve-fitted. The phase shift and backward scattering amplitude functions of Pd–Pd and Pd–Cl were extracted from Pd metal and PtCl_2 using the FEFF8 program.

3. Results and discussion

3.1. Morphology and structure of Pd/ Ga_2O_3 photocatalysts

We performed XRD measurement to analyze crystalline components of Pd(PD)/ Ga_2O_3 powder. The XRD pattern exhibited the peaks assigned to $\beta\text{-Ga}_2\text{O}_3$ (Powder Diffraction File 01–087-1901) (Fig. S2). The diffraction peak of Pd metal was not confirmed for 0.1 wt% and 0.5 wt% Pd(PD)/ Ga_2O_3 . This is due to the high dispersion of Pd and the overlapping with Ga_2O_3 peaks.

We observed the morphology of Pd(PD)/ Ga_2O_3 particles by SEM and TEM. The SEM image of 0.5 wt% Pd(PD)/ Ga_2O_3 shows the large

Ga_2O_3 particles with a width of 500 nm to 1 μm and a length of 2–4 μm (Fig. S3). The backscattered electron detector (BED) image, which shows the difference in the elemental composition, indicates the presence of Pd particles as bright spots with a size of several tens of nanometers or less. TEM images of 0.5 wt% Pd(PD)/ Ga_2O_3 revealed that the photodeposited Pd particles were about 10–20 nm in diameter (Fig. S4).

We performed Pd K-edge XAFS measurement to investigate the difference in the chemical state of the Pd cocatalysts prepared by the photodeposition and the impregnation methods. The X-ray absorption near edge structure (XANES) spectrum of 0.5 wt% Pd (PD)/ Ga_2O_3 shows that the photodeposited Pd species was in a metallic state (Fig. S5). On the other hand, the XANES spectrum of Pd(Imp)/ Ga_2O_3 was similar to PdCl_2 . Similar results were obtained from extended X-ray absorption fine structure (EXAFS) analysis (Fig. S6). The results of the curve fitting of the EXAFS spectra are summarized in Table S1. The coordination number of Pd–Pd bonds was 9.7 for Pd(PD)/ Ga_2O_3 . In the case of Pd(Imp)/ Ga_2O_3 , Pd–Pd bonds were hardly observed, and the coordination number of Pd–Cl bonds was 3.8, indicating that the local structure of the impregnated Pd species is like PdCl_2 .

3.2. Effect of cocatalyst on the photocatalytic activity

The photocatalytic CH_4 conversion was investigated for 0.1 wt% Pt(Imp)/ Ga_2O_3 and Pd(Imp)/ Ga_2O_3 prepared by the impregnation method. Fig. 1 shows the time course of at $P_{\text{CH}_4} = 98 \text{ kPa}$ and $P_{\text{H}_2\text{O}} = 3.3\text{--}3.6 \text{ kPa}$ under UV irradiation. For Pt(Imp)/ Ga_2O_3 , the amount of CO_2 produced was higher than that of C_2H_6 , suggesting that photo-SRM proceeded predominantly. On the other hand, C_2H_6 was produced more than CO_2 for Pd(Imp)/ Ga_2O_3 . The selectivity to C_2H_6 calculated on a molar carbon basis was 75.8%, which was much higher than $S_{\text{C}_2\text{H}_6}$ of Pt(Imp)/ Ga_2O_3 , indicating that Pd is a more suitable cocatalyst for C_2H_6 production than Pt. In the photocatalytic CH_4 conversion on Pd(Imp)/ Ga_2O_3 , CO and a small amount of C_3H_8 was detected as byproducts. We also confirmed the corresponding decrease of CH_4 inlet under photoirradiation (Fig. S7), indicating that CH_4 is a carbon source of C_2H_6 and CO_2 .

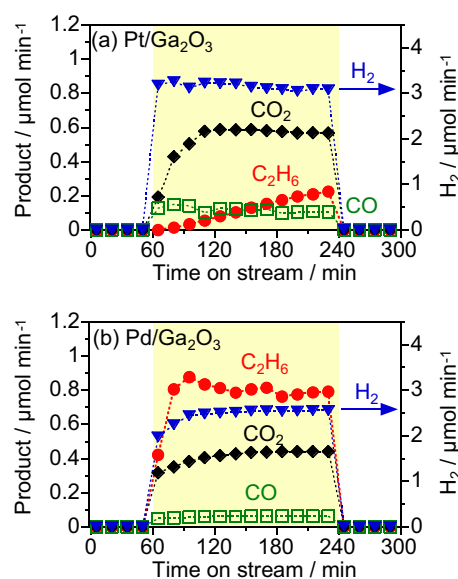


Fig. 1. Time course of the production rate in the photocatalytic conversion of CH_4 ($P_{\text{CH}_4} = 98 \text{ kPa}$) with H_2O vapor: (a) 0.1 wt% Pt(Imp)/ Ga_2O_3 ($P_{\text{H}_2\text{O}} = 3.3 \text{ kPa}$), (b) 0.1 wt% Pd(Imp)/ Ga_2O_3 ($P_{\text{H}_2\text{O}} = 3.6 \text{ kPa}$). Photoirradiation (14 mW cm^{-2}) was performed for 60–240 min on stream. The reactor temperature was set to $25 \text{ }^\circ\text{C}$. The total flow rate was 20 mL min^{-1} .

We compared the impregnation and the photodeposition methods to examine the effect of Pd cocatalyst loading. Fig. 2 shows the CH₄ conversion time course for 0.5 wt% Pd(Imp)/Ga₂O₃ and Pd(PD)/Ga₂O₃. There was an induction period in the photocatalytic product formation for Pd(Imp)/Ga₂O₃ since the initial oxidation state is Pd²⁺ species. UV–visible diffuse reflection spectra revealed that PdCl₂-like species in Pd(Imp)/Ga₂O₃ was reduced to Pd⁰ during the reaction (Fig. S8). This suggests that photoexcited electrons reduce the Pd species at the beginning of light irradiation, and the Pd metal particles exit during the photocatalytic reaction. In the case of 0.1 wt% Pd loading, there was no induction period in the photocatalytic reaction (Figure S9), suggesting the fast reduction of the supported PdCl₂-like species. The Pd(Imp)/Ga₂O₃ with in-situ formed Pd⁰ species showed $R_{C_2H_6}$ slightly higher than Pd(PD)/Ga₂O₃.

Fig. 3 shows the effect of Pd cocatalyst loading on the product formation over Pd(Imp)/Ga₂O₃ after 3-h photoirradiation. The bare Ga₂O₃ shows the low H₂ and CO₂ production rate, suggesting that photo-SRM is sluggish in the absence of Pd cocatalyst. The Pd cocatalyst significantly enhanced the reaction rate of photo-SRM and also the formation of C₂H₆. The rate of H₂ production (R_{H_2}) was significantly increased by loading a few Pd (less than 0.1 wt%), suggesting that metallic Pd cocatalyst provides a catalytic site for H₂ production. The CO₂ formation rate (R_{CO_2}) was not dependent on the Pd loading when the amount is higher than 0.025 wt%. On the other hand, the $R_{C_2H_6}$ was gradually increased with the Pd loading, indicating that the Pd cocatalyst also affects the selectivity on the oxidative reaction side. The $R_{C_2H_6}$ and $S_{C_2H_6}$ were 0.89 $\mu\text{mol min}^{-1}$ and 81.7% for 0.5 wt% Pd(Imp)/Ga₂O₃.

3.3. Effect of water vapor on the photocatalytic reaction

We investigated the effect of adding water vapor on the CH₄ conversion on a 0.1 wt% Pd(Imp)/Ga₂O₃ photocatalyst. Fig. 4 shows the time course of photocatalytic reactions in the CH₄ stream at different P_{H_2O} (0.1–3.6 kPa). In the case of $P_{H_2O} = 2.9$ kPa, the production rate was degraded after 1-h photoirradiation. The details of this degradation will be discussed in the following sections. The effect of P_{H_2O} on each product's formation rate after 3-h photoirra-

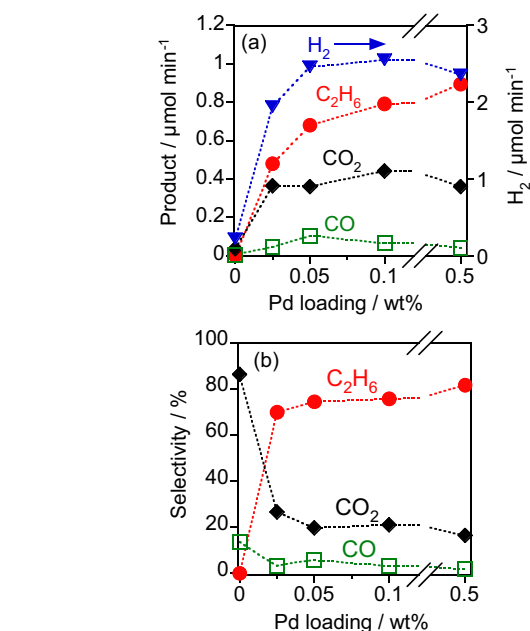


Fig. 3. Effect of Pd loading amount for Pd(Imp)/Ga₂O₃ on (a) the production rate at 3-h photoirradiation and (b) the carbon-based selectivity in the photocatalytic CH₄ conversion with H₂O vapor ($P_{CH_4} = 98$ kPa, $P_{H_2O} = 3.0$ –3.6 kPa, Temperature = 25 °C, Flow rate = 20 mL min⁻¹, Light intensity = 14 mW cm⁻²).

diation is summarized in Figure S10. Under the NOCM conditions without the oxidant ($P_{H_2O} = 0.09$ kPa), photocatalytic activity was very low since photo-SRM is difficult in the absence of water vapor. The addition of water vapor ($P_{H_2O} = 1.5$ kPa) increase R_{H_2} and R_{CO_2} due to the progress of photo-SRM. We also found a significant increase of $R_{C_2H_6}$ by water vapor, indicating that water molecule is useful not only for photo-SRM but also for C₂H₆ production (apparently NOCM).

The CO as a byproduct was detected under the conditions of $P_{H_2O} \geq 2.9$ kPa (Fig. 4d). The CO production from CH₄ can be expressed by steam reforming of methane (SRM: CH₄ + H₂O → CO +

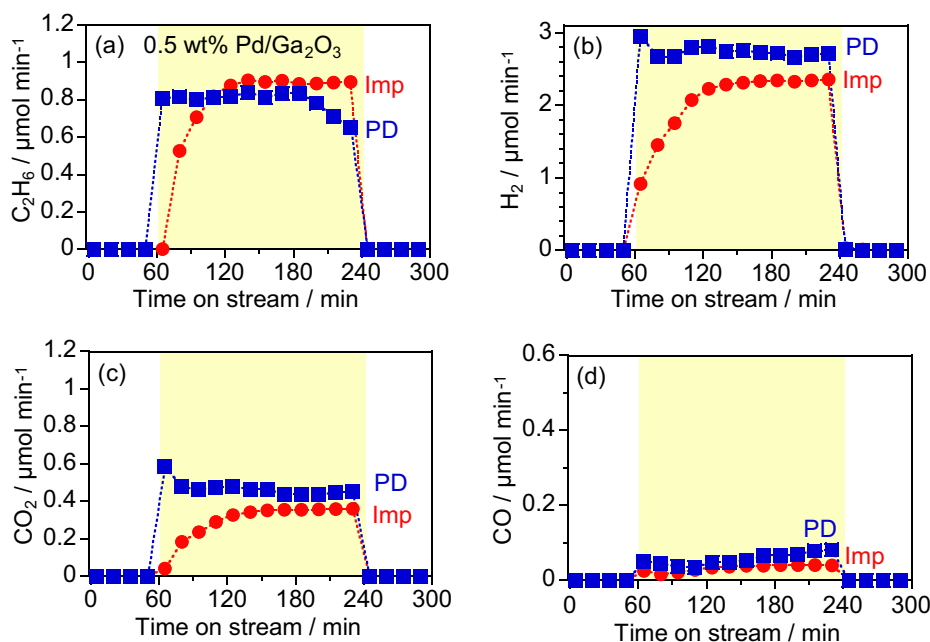


Fig. 2. Time course of the production rate of (a) C₂H₆, (b) H₂, (c) CO₂, and (d) CO in the photocatalytic CH₄ conversion on 0.5 wt% Pd(Imp)/Ga₂O₃ and Pd(PD)/Ga₂O₃ with H₂O vapor ($P_{CH_4} = 98$ kPa, $P_{H_2O} = 3.3$ kPa, Temperature = 25 °C, Flow rate = 20 mL min⁻¹, Photoirradiation 60–240 min, Light intensity = 14 mW cm⁻²).

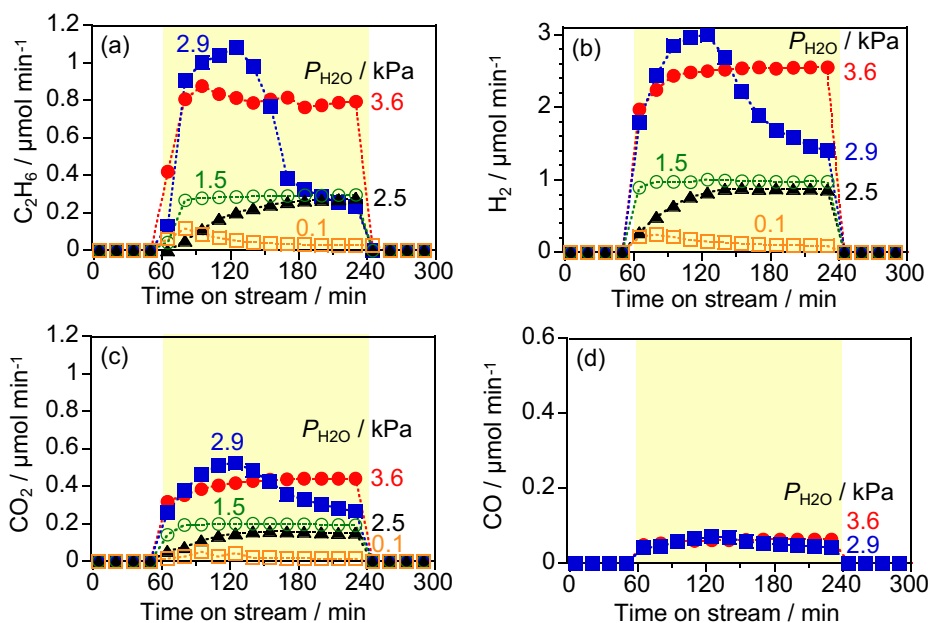


Fig. 4. Effect of $P_{\text{H}_2\text{O}}$ on the production rate of (a) C_2H_6 , (b) H_2 , (c) CO_2 , and (d) CO in the photocatalytic CH_4 conversion on 0.1 wt% Pd(Imp)/ Ga_2O_3 with H_2O vapor ($P_{\text{CH}_4} = 98$ –101 kPa, $P_{\text{H}_2\text{O}} = 0.1$ –3.6 kPa, Temperature = 25 °C, Flow rate = 20 mL min^{-1} , Photoirradiation 60–240 min, Light intensity = 14 mW cm^{-2}).

3H_2) defined in an industrial catalytic process. We evaluated the material balance between the reduction product of H_2 and the oxidation products, assuming that C_2H_6 , CO , and CO_2 are derived from the dehydrogenation of CH_4 (Fig. S11). The quantitative error was less than 10% at $P_{\text{H}_2\text{O}} \geq 1.5$ kPa, guaranteeing few missing products. The photocatalytic CH_4 conversion over 0.1 wt% Pd(Imp)/ Ga_2O_3 can be expressed in the combination of three reactions: NOCM, SRM to evolve CO_2 , and SRM to evolve CO . Noted that thermogravimetry differential thermal analysis (TG-DTA) of the photocatalyst after the reaction indicates that there is a trace amount of carbon deposition on the surface of the used photocatalyst (Fig. S11).

The product time courses (Fig. 4) showed characteristic behavior at $P_{\text{H}_2\text{O}} = 2.9$ kPa. The $R_{\text{C}_2\text{H}_6}$ was high at the initial stage (60–120 min on stream) but decreased to $0.23 \mu\text{mol min}^{-1}$ after 3-h photoirradiation. To investigate the cause of this deactivation, we conducted a stepwise reaction by changing $P_{\text{H}_2\text{O}}$ after the reaction at 2.9 kPa. Fig. 5 shows the time course when the deactivated photocatalyst was repeatedly used at $P_{\text{H}_2\text{O}} = 3.6$ kPa. The degradation was observed at $P_{\text{H}_2\text{O}} = 2.9$ kPa like in Fig. 4, but the production rate was recovered when $P_{\text{H}_2\text{O}}$ was changed to 3.6 kPa. The result indi-

cates that the cause of deactivation at $P_{\text{H}_2\text{O}} = 2.9$ kPa is not the irreversible deactivation of the Pd/ Ga_2O_3 photocatalyst but the reversible change in the reaction field. This phenomenon might be related to the amount of water vapor adsorbed on the surface, which is dependent on $P_{\text{H}_2\text{O}}$. The production rate was very stable at the relative humidity (RH) close to 100% ($P_{\text{H}_2\text{O}} = 3.6$ kPa at 27 °C). The temperature inside the reactor was increased to 27 °C under UV irradiation even though the electric cooler temperature was set to 25 °C.

In the case of 0.1 wt% Pd(Imp)/ Ga_2O_3 photocatalyst, the AQE for H_2 evolution was 11.6% at $P_{\text{H}_2\text{O}} = 3.6$ kPa, and the $S_{\text{C}_2\text{H}_6}$ was 75.8% on carbon basis. The $R_{\text{C}_2\text{H}_6}$ reached $951 \mu\text{mol g}^{-1} \text{h}^{-1}$ ($0.793 \mu\text{mol min}^{-1}$ for 50 mg photocatalyst). The high performance was stable only at high RH, suggesting that the state of water adsorbed on the surface was related to the reaction field of the Pd/ Ga_2O_3 photocatalyst. To investigate the amount of water adsorbed, we measured the water vapor adsorption and desorption isotherm of Ga_2O_3 powder at 25 °C (Fig. S12). The amount of water adsorbed on the Ga_2O_3 surface was increased with an increase in the $P_{\text{H}_2\text{O}}$. The adsorbed amount was significantly increased at $P_{\text{H}_2\text{O}} = 2.9$ kPa (RH = 91%). This type II isotherm is characteristic of multi-layer adsorption in non-porous materials [25]. The amount of water adsorbed at $P_{\text{H}_2\text{O}} = 2.9$ kPa was $12.8 \text{ cm}^3 \text{ g}^{-1}$ as an ideal gas under standard conditions (0 °C, 1 atm). Since the S_{BET} of Ga_2O_3 was $9.9 \text{ m}^2 \text{ g}^{-1}$, the water molecules adsorbed was $3.5 \times 10^{15} \text{ cm}^{-2}$. The number of water molecules in one monolayer is about $1 \times 10^{15} \text{ cm}^{-2}$ calculated from liquid water density. Therefore, approximately 3.5 monolayers (about 1 nm thickness) are formed on Ga_2O_3 at $P_{\text{H}_2\text{O}} = 2.9$ kPa and 25 °C. The multilayered water molecules with nanometer-scale thickness were necessary to induce stable CH_4 conversion on the Pd/ Ga_2O_3 photocatalyst's surface.

3.4. Effect of reaction temperature on water adsorption

In general, the amount of water adsorption decreases at high temperatures and increases at low temperatures. Therefore, the amount of water adsorbed on the Pd/ Ga_2O_3 surface can be controlled by changing the reactor temperature. Consequently, we

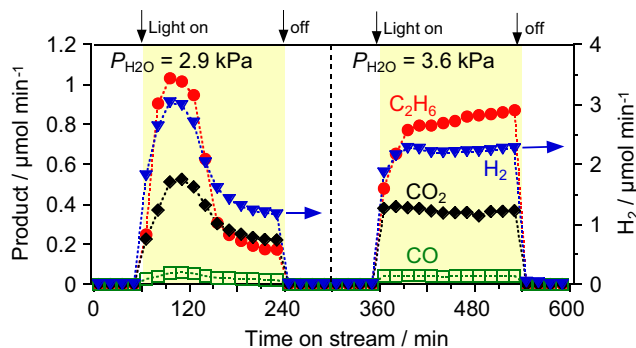


Fig. 5. Time course of the photocatalytic CH_4 conversion on 0.1 wt% Pd(Imp)/ Ga_2O_3 with different H_2O vapor pressure ($P_{\text{CH}_4} = 97$ –98 kPa, $P_{\text{H}_2\text{O}} = 2.9$ and 3.6 kPa, Temperature = 25 °C, Flow rate = 20 mL min^{-1} , Light intensity = 14 mW cm^{-2}). Photoirradiation was performed for 60–240 min and 360–540 min on stream. $P_{\text{H}_2\text{O}}$ was changed from 2.9 kPa to 3.6 kPa at 300 min on stream.

investigated the effect of reactor temperature on the photocatalytic CH_4 conversion reaction. The time courses on a 0.1 wt% Pd(imp)/ Ga_2O_3 photocatalyst are shown in Fig. S13. Fig. 6 shows each product's formation rate after 3-h photoirradiation as a function of the reaction temperature. The $R_{\text{C}_2\text{H}_6}$ was maximized at room temperature (25 °C), and decreased as the temperature increased. The $R_{\text{C}_2\text{H}_6}$ dropped significantly to $0.05 \mu\text{mol min}^{-1}$ at 65 °C. Yoshida et al. reported thermal acceleration of electron migration in Ga_2O_3 photocatalysis at temperatures less than 70 °C [19]. Therefore, the e^-h^+ recombination is not the reason for the decreased $R_{\text{C}_2\text{H}_6}$. The decreased activity would be due to the decrease in the amount of reactants adsorbed on the Ga_2O_3 photocatalyst at higher temperatures.

To investigate the change in the amount of reactants adsorbed, we performed diffuse reflectance FT-IR measurement of the Ga_2O_3 powder at different temperatures (Fig. 7). The FT-IR spectra were recorded for the powder under the CH_4 flow with water vapor of 3.0 kPa. The absorption peak with a wavenumber of 3010 cm^{-1} is assigned to the CH stretching vibration of CH_4 in the gas phase. The adsorption of CH_4 is very weak at around room temperature. On the other hand, we observed broad absorption bands at 3460 cm^{-1} and 1636 cm^{-1} due to the adsorbed water. These bands are attributed to the OH stretching vibration (3460 cm^{-1}) and the H–O–H bending vibration (1636 cm^{-1}) of the hydrogen-bonded water molecules, respectively [26,27]. Increasing the temperature from 25 °C to 65 °C decreased the intensity of the OH stretching and H–O–H bending bands. This result indicates that the amount of water adsorbed on the Ga_2O_3 photocatalyst decreases when the reaction temperature is higher than room temperature. Therefore, we can conclude that the decrease in photocatalytic activity at 35 and 65 °C is due to the decrease in the adsorbed water.

When the photocatalytic reaction was performed at low temperature (15 °C), $R_{\text{C}_2\text{H}_6}$ was decreased to $0.40 \mu\text{mol min}^{-1}$ (Fig. 6). The saturated water vapor pressure at a temperature of 15 °C is 1.7 kPa [23]. Therefore, part of the water vapor condenses when 3.0 kPa of water vapor is continuously supplied to the reactor cooled to 15 °C. In fact, we observed that water droplets were formed in the reactor, and the Pd/ Ga_2O_3 powder was wetted after the reaction. This suggests that the thick layer of liquid water formed on the Pd/ Ga_2O_3 surface negatively affects the photocatalytic activity. The solubility of hydrophobic CH_4 in water is as low as 1.6 mmol L^{-1} , and the diffusion coefficient in water is very small ($0.0018 \text{ mm}^2 \text{ s}^{-1}$) [28]. On the other hand, the concentration of CH_4 in the gas phase is 41 mmol L^{-1} , and the diffusion coefficient ($21 \text{ mm}^2 \text{ s}^{-1}$) is high in the air. This supports the hypothesis that the thick water layer prevents the supply of CH_4 to the photocatalyst surface, resulting in low photocatalytic activity.

To confirm the effect of liquid water, we carried out photocatalytic reactions using 0.1 wt% Pd(imp)/ Ga_2O_3 powder wetted with 200 μL of water droplets (Fig. S14). The $R_{\text{C}_2\text{H}_6}$ was significantly

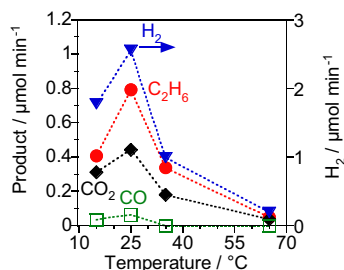


Fig. 6. Effect of reaction temperature on the production rate in the photocatalytic CH_4 conversion on 0.1 wt% Pd(imp)/ Ga_2O_3 with H_2O vapor ($P_{\text{CH}_4} = 97\text{--}98 \text{ kPa}$, $P_{\text{H}_2\text{O}} = 3.0\text{--}3.7 \text{ kPa}$, Temperature = 15–65 °C, Flow rate = 20 mL min^{-1} , Light intensity = 14 mW cm^{-2}). The data was obtained after 3-h photoirradiation.

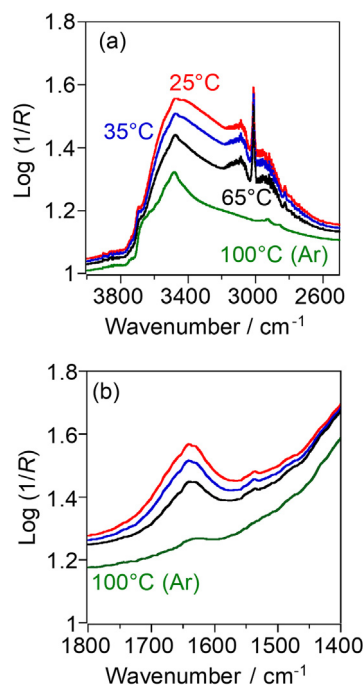


Fig. 7. Diffuse reflectance FT-IR spectra of Ga_2O_3 powders under the stream of CH_4 with H_2O vapor ($P_{\text{CH}_4} = 98 \text{ kPa}$, $P_{\text{H}_2\text{O}} = 3.0 \text{ kPa}$) at different temperatures (25–65 °C). (a) OH stretching band region of $4100\text{--}2500 \text{ cm}^{-1}$, and (b) OH deformation vibration band region of $1800\text{--}1400 \text{ cm}^{-1}$. The green curve was obtained under dry Ar stream at 100 °C. (For interpretation of the references to colour in this figure legend, the reader is referred to the web version of this article.)

decreased to $0.08 \mu\text{mol min}^{-1}$ in the presence of liquid water. The addition of water droplets to Pd/ Ga_2O_3 powder also decreased R_{CO} and R_{H_2} . On the other hand, the R_{CO_2} was not affected by the presence of liquid water. Therefore, the CO_2 selectivity was increased by the formation of a thick water layer. This is because hydrophobic CH_4 is difficult to approach the photocatalyst surface covered with liquid water, meanwhile the amount of hydroxy radical ($\bullet\text{OH}$) is constant. The $\bullet\text{OH}$, which is produced by one-electron oxidation of water molecule by photogenerated h^+ , has strong oxidizing power for organic compounds and is known as an active species for photocatalytic oxidative decomposition into CO_2 [29–31]. When the CH_4 supply to the Ga_2O_3 surface is slowed down, the surface concentration of $\bullet\text{OH}$ will increase. The excessive $\bullet\text{OH}$ promotes sequential oxidation of CH_4 into CO_2 . The active species for one-electron oxidation of CH_4 to produce $\bullet\text{CH}_3$ is assumed to be $\bullet\text{OH}$ (Equation 4). To prove the formation of $\bullet\text{OH}$, we conducted EPR spin-trapping technique with DMPO (Figure S15). The signal observed under UV irradiation was consistent to the reported 1:2:2:1 quartet spectrum for DMPO-OH spin adduct ($g = 2.005$, $A_N = 1.49 \text{ mT}$, $A_H = 1.49 \text{ mT}$) [32,33]. The A_N and A_H are hyperfine splittings of the N and $\beta\text{-H}$ atoms of the DMPO-OH adduct. The $\bullet\text{OH}$ to convert CH_4 to C_2H_6 would be generated in the water layer adsorbed on Pd/ Ga_2O_3 surface (Figure S16). On the other hand, the complete oxidation to CO_2 is promoted when the surface concentration of $\bullet\text{OH}$ is much higher than the supply of CH_4 to the surface.

3.5. Effect of other conditions on the photocatalytic reaction

We investigated the effect of total pressure on the photocatalytic CH_4 conversion over 0.1 wt% Pd(imp)/ Ga_2O_3 photocatalyst (Fig. 8). When the total pressure was 1 atm or less, $R_{\text{C}_2\text{H}_6}$ and R_{H_2} increased with P_{CH_4} . However, the increasing trend of $R_{\text{C}_2\text{H}_6}$ was not clear at $P_{\text{CH}_4} \geq 100 \text{ kPa}$ or more. This result is different from

the result observed for Pt/Ga₂O₃ photocatalyst; The $R_{C_2H_6}$ is monotonously increased up to $P_{CH_4} = 300$ kPa when Pt is cocatalyst [20]. The $R_{C_2H_6}$ on Pd/Ga₂O₃ was $0.64 \mu\text{mol min}^{-1}$ at $P_{CH_4} = 50$ kPa, which was much higher than $0.10 \mu\text{mol min}^{-1}$ for Pt/Ga₂O₃ at the same condition [20]. Therefore, we can conclude that Pd/Ga₂O₃ is an excellent photocatalyst for selective C₂H₆ production even at low P_{CH_4} in the presence of water vapor. The highest $S_{C_2H_6}$ (75.8%) was observed at $P_{CH_4} = 100$ kPa since CO₂ selectivity slightly decreased at high P_{CH_4} . We understand that this is because high P_{CH_4} increased the surface concentration of $\bullet\text{CH}_3$, promoting coupling into C₂H₆.

Fig. 9 shows the effect of incident light intensity for 0.1 wt% Pd (Imp)/Ga₂O₃ photocatalyst. The R_{CO_2} increased linearly with light intensity. $R_{C_2H_6}$ also increased with increasing light intensity, but the increase became gradual at above 5 mW cm^{-2} . As a result, the $S_{C_2H_6}$ was slightly decreased as the light intensity increased. When the light intensity is high, the high density $\bullet\text{OH}$ promotes the sequential oxidation into CO₂. This implies that a moderate concentration of surface $\bullet\text{OH}$ species is required for highly selective NOCM. The highest $S_{C_2H_6}$ of 81.5% was observed at low light intensity (5 mW cm^{-2}) for 0.1 wt% Pd(Imp)/Ga₂O₃.

Fig. 10 shows the effect of the feed gas flow rate on the photocatalytic reaction over 0.1 wt% Pd(Imp)/Ga₂O₃. We calculated the conversion rate of CH₄ from the ratio of each production rate ($R_{C_2H_6}$, R_{CO_2} , R_{CO}) to the flow rate of the CH₄ inlet. The formation rates of each product were constant during photoirradiation. The $R_{C_2H_6}$ was remarkably increased when the CH₄ flow rate was increased. The $R_{C_2H_6}$ was $1.11 \mu\text{mol min}^{-1}$, the $S_{C_2H_6}$ was 80.4%, and AQE for H₂ evolution was 14.4% at the flow rate of 30 mL min^{-1} . The AQE for C₂H₆ and CO₂ was 5.1% and 8.8% assuming a two-electron process ($2\text{CH}_4 + 2 \text{h}^+ \rightarrow \text{C}_2\text{H}_6 + 2\text{H}^+$) and an eight-electron process ($\text{CH}_4 + 2\text{H}_2\text{O} + 8 \text{h}^+ \rightarrow \text{CO}_2 + 8\text{H}^+$), respectively. When the CH₄ flow rate was 40 mL min^{-1} , $R_{C_2H_6}$ was saturated, but $S_{C_2H_6}$ reached a maximum of 83.3%. The $R_{C_2H_6}$ enhanced by the increased flow rate is probably because of the improvement

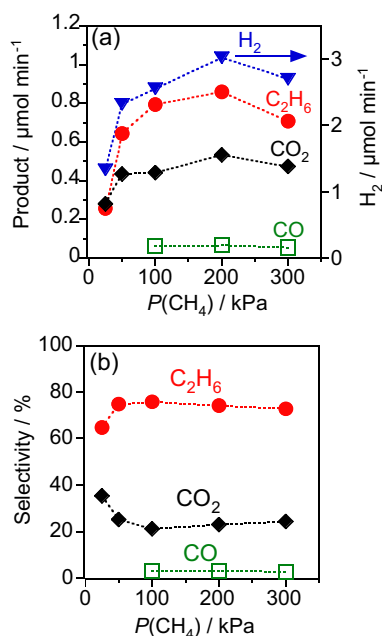


Fig. 8. Effect of P_{CH_4} on (a) the production rate after 3-h photoirradiation and (b) the carbon-based selectivity in the photocatalytic CH₄ conversion on 0.1 wt% Pd (Imp)/Ga₂O₃ with H₂O vapor ($P_{CH_4} = 25$ –300 kPa, $P_{H_2O} = 3.5$ –3.7 kPa, Temperature = 25 °C, Flow rate = 20 mL min^{-1} , Light intensity = 14 mW cm^{-2}). Argon was used as a balance gas when total pressure was less than 101 kPa. The pressure higher than 101 kPa was regulated by a back-pressure valve.

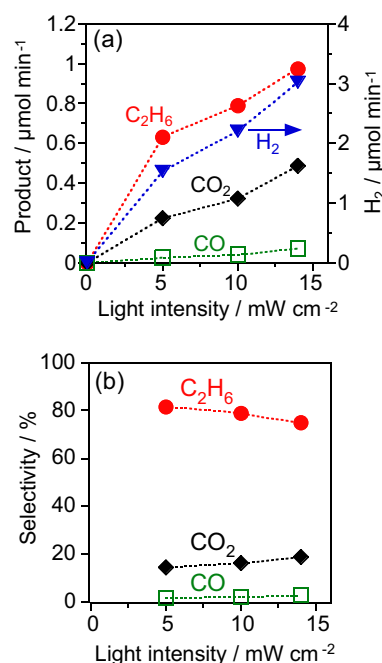


Fig. 9. Effect of light intensity on the production rate in the photocatalytic CH₄ conversion on 0.1 wt% Pd(Imp)/Ga₂O₃ with H₂O vapor ($P_{CH_4} = 98$ kPa, $P_{H_2O} = 3.6$ kPa, Temperature = 25 °C, Flow rate = 20 mL min^{-1} , Light intensity = 5.0 – 14 mW cm^{-2}). The data were obtained after 3-h photoirradiation.

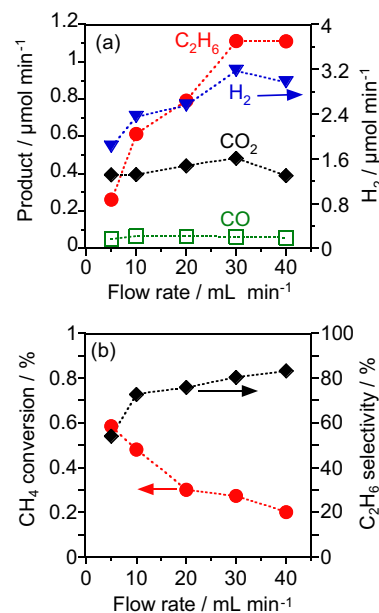


Fig. 10. Effect of flow rate of CH₄ on (a) the production rate after 3-h photoirradiation and (b) the CH₄ conversion and the C₂H₆ selectivity in the photocatalytic CH₄ conversion on 0.1 wt% Pd(Imp)/Ga₂O₃ with H₂O vapor ($P_{CH_4} = 97$ –98 kPa, $P_{H_2O} = 3.2$ –3.7 kPa, Temperature = 25 °C, Flow rate = 5 – 40 mL min^{-1} , Light intensity = 14 mW cm^{-2}).

in the diffusivity of $\bullet\text{CH}_3$ on the photocatalyst surface to suppress the sequential decomposition. On the other hand, $S_{C_2H_6}$ decreased with the promotion of CO₂ formation when the flow rate was set to 5 mL min^{-1} . This suggests that the sequential oxidations by $\bullet\text{OH}$ is easily promoted at the slow flow rate. The CH₄ conversion rate was 0.58% when the flow rate was 5 mL min^{-1} , although the $S_{C_2H_6}$ was not high.

4. Conclusion

In this study, we investigated the characteristics of the Pd/Ga₂O₃ photocatalyst for CH₄ conversion reaction in the presence of water vapor. Pd/Ga₂O₃ was effective for selective C₂H₆ formation compared with Pt/Ga₂O₃. The production rate of C₂H₆ was larger when the PdCl₂-like species was initially loaded by the impregnation method. The Pd species are reduced to a metallic state, which is the site promoting H₂ production, during the photocatalytic reaction.

We investigated the effect of adding water vapor on the C₂H₆ formation rate over the Pd/Ga₂O₃ photocatalyst. When water was not added, the amount of C₂H₆ produced was very small. However, steady C₂H₆ formation ($R_{C_2H_6} = 0.79 \mu\text{mol min}^{-1}$) was confirmed at $P_{H_2O} = 3.6 \text{ kPa}$. The AQE for H₂ production was 11.6%, and the selectivity of C₂H₆ was 75.8% on a carbon basis. The photocatalytic activity was reversibly affected by the P_{H_2O} . Also, $R_{C_2H_6}$ decreased significantly under the conditions for condensation of water vapor to liquid water. The presence of water vapor close to the saturated water vapor pressure was necessary for inducing the photocatalytic dehydrogenative coupling of CH₄ to produce C₂H₆ and H₂.

We evaluated the adsorbed water on the photocatalyst surface by measuring the adsorption isotherm of water vapor and In-situ FT-IR spectroscopy. The water molecules adsorbed on the surface provides a reaction field promoting C₂H₆ production. The multilayered water molecules with a thickness of about 1 nm (3.5 monolayers) facilitate the reaction based on the following mechanisms: 1) increasing the amount of •OH, which activates CH₄ to •CH₃, 2) preventing the sequential oxidative decomposition of the •CH₃ by •OH, and 3) increasing the homocoupling of •CH₃ to C₂H₆. The dependence on the C₂H₆ production rate on the light intensity and the flow rate implies that CO₂ formation is accelerated when •OH is excessively generated, and C₂H₆ is easily produced when the diffusivity of the •CH₃ is improved. These new insights on a hydrophilic reaction field advance the surface engineering controlling the photocatalysis for CH₄ conversion.

The Pd/Ga₂O₃ photocatalyst shows high efficiency for H₂ production (AQE = 14.4%) and the C₂H₆ selectivity higher than 80% at a CH₄ flow rate of 30 mL min⁻¹. The developed photocatalytic system was much better than previously reported ones for NOCM in the absence of water vapor. However, the CH₄ conversions in the flow reactor were still low at the industrial level. Therefore, it is necessary to improve the CH₄ conversion rate further while maintaining high selectivity for C₂H₆ in the photocatalytic system.

Declaration of Competing Interest

The authors declare that they have no known competing financial interests or personal relationships that could have appeared to influence the work reported in this paper.

Acknowledgment

This work was supported by JST PRESTO [grant number JPMJPR18T1] and JSPS KAKENHI [grant number JP20H02525]. The synchrotron radiation experiment was performed under the approval of the Japan Synchrotron Radiation Research Institute (JASRI) as 2020A1410.

Appendix A. Supplementary data

Supplementary data to this article can be found online at <https://doi.org/10.1016/j.jcat.2021.03.024>.

References

- [1] S.Y. Lee, G.D. Holder, Methane hydrates potential as a future energy source, *Fuel Process. Technol.* 71 (2001) 181–186, [https://doi.org/10.1016/S0378-3820\(01\)00145-X](https://doi.org/10.1016/S0378-3820(01)00145-X).
- [2] J. Baltrusaitis, I. Jansen, J.D. Schuttlefield Christus, Renewable energy based catalytic CH₄ conversion to fuels, *Catal. Sci. Technol.* 4 (2014) 2397–2411, <https://doi.org/10.1039/c4cy00294f>.
- [3] H. Song, X. Meng, Z. Wang, H. Liu, J. Ye, Solar-Energy-Mediated Methane Conversion, *Joule*. 3 (2019) 1606–1636, <https://doi.org/10.1016/j.joule.2019.06.023>.
- [4] W. Taifan, J. Baltrusaitis, CH₄ conversion to value added products: Potential, limitations and extensions of a single step heterogeneous catalysis, *Appl. Catal. B Environ.* 198 (2016) 525–547, <https://doi.org/10.1016/j.apcatb.2016.05.081>.
- [5] Y. Gambo, A.A. Jalil, S. Triwahyono, A.A. Abdulrasheed, Recent advances and future prospect in catalysts for oxidative coupling of methane to ethylene: A review, *J. Ind. Eng. Chem.* 59 (2018) 218–229, <https://doi.org/10.1016/j.jiec.2017.10.027>.
- [6] P. Schwach, X. Pan, X. Bao, Direct Conversion of Methane to Value-Added Chemicals over Heterogeneous Catalysts: Challenges and Prospects, *Chem. Rev.* 117 (2017) 8497–8520, <https://doi.org/10.1021/acs.chemrev.6b00715>.
- [7] X. Cao, T. Han, Q. Peng, C. Chen, Y. Li, Modifications of heterogeneous photocatalysts for hydrocarbon C-H bond activation and selective conversion, *Chem. Commun.* 56 (2020) 13918–13932, <https://doi.org/10.1039/d0cc05785a>.
- [8] A. Kudo, Y. Miseki, Heterogeneous photocatalyst materials for water splitting, *Chem. Soc. Rev.* 38 (2009) 253–278, <https://doi.org/10.1039/b800489g>.
- [9] K. Shimura, H. Yoshida, Semiconductor Photocatalysts for Non-oxidative Coupling, Dry Reforming and Steam Reforming of Methane, *Catal. Surv. from Asia*. 18 (2014) 24–33, <https://doi.org/10.1007/s10563-014-9165-z>.
- [10] L. Yuliaty, H. Yoshida, Photocatalytic conversion of methane, *Chem. Soc. Rev.* 37 (2008) 1592–1602, <https://doi.org/10.1039/b710575b>.
- [11] F. Amano, A. Shintani, K. Tsurui, H. Mukohara, T. Ohno, S. Takenaka, Photoelectrochemical Homocoupling of Methane under Blue Light Irradiation, *ACS Energy Lett.* 4 (2019) 502–507, <https://doi.org/10.1021/acscenergylett.8b02436>.
- [12] W. Li, D. He, G. Hu, X. Li, G. Banerjee, J. Li, S.H. Lee, Q. Dong, T. Gao, G.W. Brudvig, M.M. Waagele, D.E. Jiang, D. Wang, Selective CO Production by Photoelectrochemical Methane Oxidation on TiO₂, *ACS Cent. Sci.* 4 (2018) 631–637, <https://doi.org/10.1021/acscentsci.8b00130>.
- [13] S. Wu, X. Tan, J. Lei, H. Chen, L. Wang, J. Zhang, Ga-Doped and Pt-Loaded Porous TiO₂-SiO₂ for Photocatalytic Nonoxidative Coupling of Methane, *J. Am. Chem. Soc.* 141 (2019) 6592–6600, <https://doi.org/10.1021/jacs.8b13858>.
- [14] X. Yu, V.L. Zholobenko, S. Moldovan, D. Hu, D. Wu, V.V. Ordomsky, A.Y. Khodakov, Stoichiometric methane conversion to ethane using photochemical looping at ambient temperature, *Nat. Energy*. 5 (2020) 511–519, <https://doi.org/10.1038/s41560-020-0616-7>.
- [15] L. Yuliaty, T. Hattori, H. Itoh, H. Yoshida, Photocatalytic nonoxidative coupling of methane on gallium oxide and silica-supported gallium oxide, *J. Catal.* 257 (2008) 396–402, <https://doi.org/10.1016/j.jcat.2008.05.022>.
- [16] J. Lang, Y. Ma, X. Wu, Y. Jiang, Y.H. Hu, Highly efficient light-driven methane coupling under ambient conditions based on an integrated design of a photocatalytic system, *Green Chem.* 22 (2020) 4669–4675, <https://doi.org/10.1039/d0gc01608j>.
- [17] S.P. Singh, A. Anzai, S. Kawaharasaki, A. Yamamoto, H. Yoshida, Non-oxidative coupling of methane over Pd-loaded gallium oxide photocatalysts in a flow reactor, *Catal. Today*. 362 (2021) in Press. <https://doi.org/10.1016/j.cattod.2020.04.023>.
- [18] K. Shimura, T. Yoshida, H. Yoshida, Photocatalytic activation of water and methane over modified gallium oxide for hydrogen production, *J. Phys. Chem. C*. 114 (2010) 11466–11474, <https://doi.org/10.1021/jp1012126>.
- [19] K. Shimura, K. Maeda, H. Yoshida, Thermal acceleration of electron migration in gallium oxide photocatalysts, *J. Phys. Chem. C*. 115 (2011) 9041–9047, <https://doi.org/10.1021/jp110824n>.
- [20] F. Amano, C. Akamoto, M. Ishimaru, S. Inagaki, H. Yoshida, Pressure-induced dehydrogenative coupling of methane to ethane by platinum-loaded gallium oxide photocatalyst, *Chem. Commun.* 56 (2020) 6348–6351, <https://doi.org/10.1039/d0cc01730b>.
- [21] L. Yu, Y. Shao, D. Li, Direct combination of hydrogen evolution from water and methane conversion in a photocatalytic system over Pt/TiO₂, *Appl. Catal. B Environ.* 204 (2017) 216–223, <https://doi.org/10.1016/j.apcatb.2016.11.039>.
- [22] L. Yu, D. Li, Photocatalytic methane conversion coupled with hydrogen evolution from water over Pd/TiO₂, *Catal. Sci. Technol.* 7 (2017) 635–640, <https://doi.org/10.1039/c6cy02435a>.
- [23] O.A. Alduchov, R.E. Eskridge, Improved Magnus form approximation of saturation vapor pressure, *Appl. Meteor.* 35 (1996) 601–609, [https://doi.org/10.1175/1520-0450\(1996\)035<0601:IMFAOS>2.0.CO;2](https://doi.org/10.1175/1520-0450(1996)035<0601:IMFAOS>2.0.CO;2).
- [24] H. Asakura, S. Yamazoe, T. Misumi, A. Fujita, T. Tsukuda, T. Tanaka, xTunes: A new XAS processing tool for detailed and on-the-fly analysis, *Radiat. Phys. Chem.* 175 (2020), <https://doi.org/10.1016/j.radphyschem.2019.04.020>.
- [25] N.C. Burtch, H. Jasuja, K.S. Walton, Water stability and adsorption in metal-organic frameworks, *Chem. Rev.* 114 (2014) 10575–10612, <https://doi.org/10.1021/cr5002589>.
- [26] K. Shirai, T. Sugimoto, K. Watanabe, M. Haruta, H. Kurata, Y. Matsumoto, Effect of water adsorption on carrier trapping dynamics at the surface of anatase TiO₂

- nanoparticles, *Nano Lett.* 16 (2016) 1323–1327, <https://doi.org/10.1021/acs.nanolett.5b04724>.
- [27] K. Shirai, G. Fazio, T. Sugimoto, D. Selli, L. Ferraro, K. Watanabe, M. Haruta, B. Ohtani, H. Kurata, C. Di Valentin, Y. Matsumoto, Water-Assisted Hole Trapping at the Highly Curved Surface of Nano-TiO₂ Photocatalyst, *J. Am. Chem. Soc.* 140 (2018) 1415–1422, <https://doi.org/10.1021/jacs.7b11061>.
- [28] J. Rumble, *CRC Handbook of Chemistry and Physics*, 100th Edit, CRC Press, Boca Raton, Florida, 2019.
- [29] A. Fujishima, T.N. Rao, D.A. Tryk, Titanium dioxide photocatalysis, *J. Photochem. Photobiol. C* 1 (2000) 1–21, [https://doi.org/10.1016/S1389-5567\(00\)00002-2](https://doi.org/10.1016/S1389-5567(00)00002-2).
- [30] Y. Nosaka, A.Y. Nosaka, Generation and Detection of Reactive Oxygen Species in Photocatalysis, *Chem. Rev.* 117 (2017) 11302–11336, <https://doi.org/10.1021/acs.chemrev.7b00161>.
- [31] C.S. Turchi, D.F. Ollis, Photocatalytic degradation of organic water contaminants: Mechanisms involving hydroxyl radical attack, *J. Catal.* 122 (1990) 178–192, [https://doi.org/10.1016/0021-9517\(90\)90269-P](https://doi.org/10.1016/0021-9517(90)90269-P).
- [32] A. Bosnjakovic, S. Schlick, Spin Trapping by 5,5-Dimethylpyrroline-N-oxide in Fenton Media in the Presence of Nafion Perfluorinated Membranes: Limitations and Potential, *J. Phys. Chem. B* 110 (2006) 10720–10728, <https://doi.org/10.1021/jp061042y>.
- [33] H. Song, X. Meng, S. Wang, W. Zhou, X. Wang, T. Kako, J. Ye, Direct and Selective Photocatalytic Oxidation of CH₄ to Oxygenates with O₂ on Cocatalysts/ZnO at Room Temperature in Water, *J. Am. Chem. Soc.* 141 (2019) 20507–20515, <https://doi.org/10.1021/jacs.9b11440>.